PERGAMON

International Journal of Solids and Structures 36 (1999) 241–268

INTERNATIONAL JOURNAL OF SOLIDS and STRUCTURES

Interactions of kinked interfacial cracks

Mao S. Wu*, Hong Zhou

Department of Engineering Mechanics, University of Nebraska-Lincoln, W317-4 Nebraska Hall, Lincoln NE 68588-0526, U.S.A.

Received 23 November 1996; in revised form 3 September 1997

Abstract

The interactions of kinked interfacial cracks between two dissimilar isotropic media subjected to remote tension are investigated in this paper. The analytical technique consists of the dislocation modeling of the kinks, and the formulation generalizes previous models for a single crack to a model for two strongly interacting cracks. For two sets of Dundurs parameters, it is shown that the dependence of the stress intensity factors and the energy release rate on the geometrical and material parameters can be very complex due to interaction and the asymmetry of the crack configuration. It is also shown that interaction can change the kinking behavior completely, and that discrepancies in the kink angle and the critical stress predictions of the maximum energy release rate and the maximum mode I stress intensity factor criteria are affected by interaction.

1. Introduction

The problem of interfacial cracks in a two-dimensional bi-material solid has been studied since the late 1950's, e.g. Williams (1959) and Rice and Sih (1965). Further references can be found in the review of Raju and Dattaguru (1995). More recently, the kinking of an interfacial crack has been investigated for dissimilar isotropic media (He and Hutchinson, 1989; Mukai et al., 1990) and for dissimilar anisotropic media (Miller and Stock, 1989). In contrast, the kinking of a crack in a homogeneous isotropic medium has been investigated at least since the 1970's (e.g. Lo, 1978). The case of a kinked crack in a homogeneous anisotropic material can be found in the comparatively recent work of Obata et al. (1989).

The above-mentioned works on crack kinking focus on a single crack. A voluminous amount of work has been done for the interactions of straight cracks in two- and three-dimensional homogeneous media, both infinite and finite. Multiple interfacial cracks also exist, for instance, due to imperfect bonding at the interface (e.g. Kang, 1994). They can be found in metal–ceramic

* Corresponding author. E-mail: wu@emwu.unl.edu.

0020–7683/99/$—see front matter
PII: S0020–7683(97)00275–8

bonded joints, adhesive joints, electronic devices, and composite materials in general. Consequently, quantitative predictions of their interactions and possible kinking is of great importance in the understanding of the degradation of materials or structural function. Attempts have been made towards the analysis of the interaction between straight interfacial cracks (e.g. Zhao and Chen, 1994) and between a straight interfacial crack and a straight subinterfacial crack (e.g. Isida and Noguchi, 1994; Zhao and Chen, 1995). To the best knowledge of the authors, investigations on the interactions of interfacial kinked cracks have not been carried out, however. Recently, Niu and Wu (1997) attempted the study of the interactions of kinked, branched and zigzag cracks in homogeneous isotropic media subjected to remote tension.

There has also been a great deal of interest in the appropriate fracture criteria for predicting kinking out of an interface. He and Hutchinson (1989) used the maximum energy release rate criterion. Miller and Stock (1989) considered the maximum mode I stress intensity factor (SIF) criterion. Similarly, Yuuki et al. (1994) considered the maximum hoop stress criterion. Kang (1994) compared the predictions of the maximum energy release rate, the maximum hoop stress and the zero mode II SIF criteria with experimental data. All these works considered a single crack. It is thus of theoretical and practical importance to investigate whether the predictions of the different criteria can be affected by the interactions between multiple kinked cracks on the interface.

This paper investigates the interactions of kinked interfacial cracks lying between two dissimilar infinite isotropic media subjected to remote tension. For simplicity, two cracks, not necessarily equal, are considered. The plane strain condition is assumed. The objectives are to (i) understand the influence of strong interactions and crack configuration asymmetry on the stress intensity factors, the energy release rate and the kink angle, and (ii) study how these factors influence the differences in the kink angle and critical stress predictions of two different fracture criteria. These are the practical contributions of the present work. The analytical technique makes use of the dislocation modeling of kinks in the manner of Lo (1978), as is the case in He and Hutchinson (1989), Obata et al. (1989), Mukai et al. (1990), and Niu and Wu (1997). The technique for treating interfacial boundary conditions follows that of England (1965) and Clements (1971), as is the case in Mukai et al. (1990). The theoretical contribution of the present work is to generalize the single interfacial kinked crack model to a model for two interfacial kinked cracks using the method of dislocations, and to emphasize that the key element responsible for the success of the method is the exact satisfaction of the boundary conditions by all the interfacial parts of the kinked cracks.

The problem is formulated in Section 2, and the potential function solutions are provided in Section 3. The integral equations associated with the kinks are developed in Section 4. Numerical results are presented in Section 5, and the conclusions in Section 6.

2. Formulation

2.1. *Problem statement*

Figure 1(a) shows an infinite body of two dissimilar isotropic media bonded along a straight interface $L+L'$ except at the two crack locations, where L is the union of the cracks and L' the union of the bonded segments. The elastic constants of the upper and lower media S_1 and S_2 are,

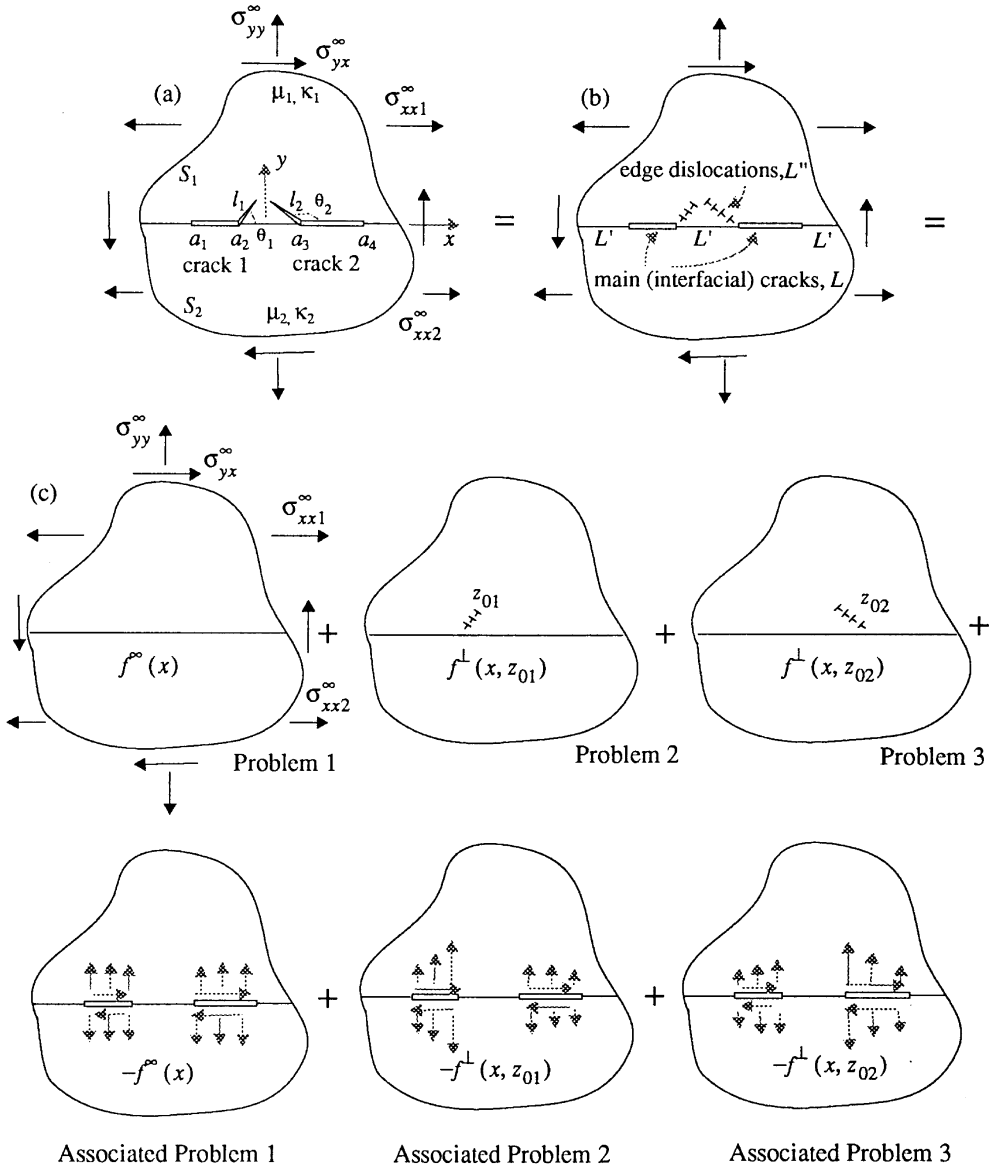

Fig. 1. Schematic of the superposition technique for solving the problem of multiple kinked interfacial cracks in a bi-material.

respectively, μ_1, κ_1 and μ_2, κ_2, where μ_j is the shear modulus and κ_j is related to the Poisson's ratio ν_j by $\kappa_j = 3-4\nu_j$ $(j = 1, 2)$ in plane strain. Denote also L'' as the union of the two straight kinks in S_j. A rectangular frame x–y is attached to the body with the x-axis lying along the interface. The interfacial parts of the cracks, or the main cracks for brevity, have their tips located at $x = a_1, a_2,$

a_3 and a_4, where $a_4 > a_3 > a_2 > a_1$. The lengths of the main cracks, labelled 1 and 2, are denoted by $2c_1 = a_2 - a_1$ and $2c_2 = a_4 - a_3$, respectively. The kinks 1 and 2 have the lengths l_1, l_2 and the angles θ_1, θ_2, respectively. The angles are measured positive counterclockwise from the x-direction. The body is subjected to the remote stresses σ^{∞}_{yy}, σ^{∞}_{yx}, σ^{∞}_{xx1} and σ^{∞}_{xx2} under plane strain. The objective is to compute the stress intensity factors (SIFs) and the energy release rate of the kinks.

2.2. *Boundary conditions*

The remote boundary conditions are specified by the remote stresses σ^{∞}_{yy} and σ^{∞}_{yx}. The x-direction stresses are related to σ^{∞}_{yy} (see Appendix A). On the interface, the stress $\sigma_{yy} - i\sigma_{yx}$ and displacement gradient $u' + iv'$ boundary conditions, where $i = \sqrt{-1}$, are:

$$(\sigma_{yy} - i\sigma_{yx})_1 - (\sigma_{yy} - i\sigma_{yx})_2 = 0 \quad \text{on } L + L', \tag{1}$$

$$(\sigma_{yy} - i\sigma_{yx})_1 = (\sigma_{yy} - i\sigma_{yx})_2 = 0 \quad \text{on } L, \tag{2}$$

and

$$(u' + iv')_1 - (u' + iv')_2 = 0 \quad \text{on } L', \tag{3}$$

where the subscripts 1 and 2 refer to S_1 and S_2, respectively. The prime on the displacement u or v denotes the derivative with respect to x. For the kinks, the stress boundary condition is:

$$\sigma_{y'y'} - i\sigma_{y'x'} = 0 \quad \text{on } L'', \tag{4}$$

where x'–y' refers to the local reference frame of either kink.

2.3. *Superposition scheme to satisfy boundary conditions*

To solve the problem in Section 2.1 subjected to the boundary conditions in Section 2.2, the superposition scheme illustrated in Fig. 1 is used. Figure 1(b) shows the replacement of the two kinks by two initially unknown distributions of infinitesimal edge dislocations. Figure 1(c) shows the decomposition of Fig. 1(b) into three problems each with its associated problem. In Problem 1, the uncracked bi-material solid is subjected to the remote stresses. In Problems 2 and 3, the uncracked body is internally stressed by the dislocations of kinks 1 and 2, respectively. Stresses are induced at the trace of the imaginary main cracks in these problems. In the associated problems, the interfacial main cracks are subjected to the negative of the induced stresses.

Superposition of the three problems and the associated problems ensures that the main cracks are traction free, i.e. (2) is satisfied. Moreover, (1) and (3) are satisfied in each of the six problems so that they are also satisfied after superposition. The remote boundary conditions are satisfied in Problem 1, and consequently no stresses should be induced at infinity in the other five problems. The potential functions in all six problems can be derived, and it remains to ensure that the kinks are traction free, see (4). The stresses on the trace of the kinks in the six problems are derived from the potentials, and setting the sum of these stresses to zero yields a system of singular integral equations containing the dislocation densities as unknown functions.

3. Potential functions

The stress and displacement fields in an infinite isotropic body can be derived from the well-known complex potentials $\Phi_j(z)$ and $\Psi_j(z)$ of Muskhelishvili (1953):

$$(\sigma_{yy}-i\sigma_{yx})_j = \Phi_j(z)+\overline{\Phi_j(z)}+z\overline{\Phi_j'(z)}+\overline{\Psi_j(z)}, \tag{5}$$

$$(\sigma_{xx}+\sigma_{yy})_j = 2[\Phi_j(z)+\overline{\Phi_j(z)}], \tag{6}$$

$$(u+iv)_j = \frac{1}{2\mu_j}\left[\kappa_j\int_0^z \Phi_j(z)\,\mathrm{d}z-\int_0^{\bar z}\bar\Psi_j(\bar z)\,\mathrm{d}\bar z-z\overline{\Phi_j(z)}\right], \tag{7}$$

where the subscript $j=1, 2$ identifies the region S_j, and $z=x+iy$ is the complex variable. Also, $\bar z$, $\overline{\Phi_j(z)}$ and $\overline{\Psi_j(z)}$ are the complex conjugates of z, $\Phi_j(z)$ and $\Psi_j(z)$, respectively, while $\bar\Psi_j(z)=\overline{\Psi_j(\bar z)}$. The prime denotes differentiation with respect to the argument of the potential. In view of (3), (7) is differentiated with respect to x:

$$(u'+iv')_j = \frac{1}{2\mu_j}[\kappa_j\Phi_j(z)-\overline{\Phi_j(z)}-z\overline{\Phi_j'(z)}-\overline{\Psi_j(z)}]. \tag{8}$$

Following England (1965), Clements (1971) and Mukai et al. (1990), the analytic potentials $\Omega_S(z)=\Omega_{Sj}(z)$ and $\Omega_D(z)=\Omega_{Dj}(z)$ where $z\in S_j$, are defined in the entire region $S=S_1+S_2$. Also, $\Omega_{Sj}(z)$ and $\Omega_{Dj}(z)$ are analytic in their respective regions. Letting $j,\ k\in\{1,2\}$ but $j\neq k$, these potentials can be defined succintly as:

$$\Omega_{Sj}(z) = \Phi_j(z)-[\bar\Phi_j(z)+z\bar\Phi_k'(z)+\bar\Psi_k(z)] \quad z\in S_j, \tag{9}$$

$$\Omega_{Dj}(z) = \frac{\kappa_j}{2\mu_j}\Phi_j(z)+\frac{1}{2\mu_k}[\bar\Phi_k(z)+z\bar\Phi_k'(z)+\bar\Psi_k(z)] \quad z\in S_j. \tag{10}$$

The conditions of stress jump $(\sigma_{yy}-i\sigma_{yx})_2-(\sigma_{yy}-i\sigma_{yx})_1$ and displacement gradient jump $(u'+iv')_2-(u'+iv')_1$ at the interface can then be conveniently expressed as $\Omega_{S2}(x)-\Omega_{S1}(x)$ and $\Omega_{D2}(x)-\Omega_{D1}(x)$, respectively. In the associated problems, these conditions on the main cracks correspond to Hilbert's problems which can be solved using the method given in Muskhelishvili (1953). The solutions $\Omega_{Sj}(z)$ and $\Omega_{Dj}(z)$ can then be used to determine $\Phi_j(z)$ and $\Psi_j(z)$ by inverting (9) and (10):

$$\Phi_j(z) = Q_j\left[\frac{1}{2\mu_k}\Omega_{Sj}(z)+\Omega_{Dj}(z)\right] \quad z\in S_j, \tag{11}$$

$$\Psi_j(z) = Q_k\left[\frac{-\kappa_k}{2\mu_k}\bar\Omega_{Sk}(z)+\bar\Omega_{Dk}(z)\right]-\Phi_j(z)-z\Phi_j'(z) \quad z\in S_j, \tag{12}$$

where $Q_j=2\mu_j\mu_k/(\mu_j+\kappa_j\mu_k)$. The potentials of the three uncracked problems, i.e. $(\Phi_j^\infty(z),\ \Psi_j^\infty(z))$ associated with the remote loading, and $(\Phi_j^\perp(z),\ \Psi_j^\perp(z))$ associated with the internal loading of the dislocations, are available in the literature and are listed in Appendix A for completeness. The potentials of the associated problems, distinguished by carets, i.e. $(\hat\Phi_j^\infty(z),\ \hat\Psi_j^\infty(z))$, $(\Phi_j^\perp(z),$

$\hat{\Psi}_j^{\perp}(z)$), ($\hat{\Omega}_{Sj}^{\infty}(z)$, $\hat{\Omega}_{Dj}^{\infty}(z)$) and ($\hat{\Omega}_{Sj}^{\perp}(z)$, $\hat{\Omega}_{Dj}^{\perp}(z)$) are derived as the solutions of Hilbert's problems in the following sub-sections.

It is emphasized that the key element responsible for the success of the present approach is the exact satisfaction of the boundary conditions on all main cracks. When the main cracks are very close to each other, it is extremely difficult to satisfy their boundary conditions and hence obtain an accurate estimate of the SIFs in the case of strong interaction. Attempts to describe the very strong interaction by approximate functions such as a series of orthogonal polynomials have met with limited success. Thus, the theoretical contribution to this work is the derivation and solution of the associated problems in such a manner that the exact satisfaction of all main crack boundary conditions under the remote or dislocation loading is guaranteed *a priori*.

3.1. *Associated Problem* 1

The potentials of Problem 1 are given in Appendix A. In Associated Problem 1 (Fig. 1(c)), the boundary conditions are the same as the overall boundary conditions given in (1)–(3), except that (2) should be replaced by $(\sigma_{yy}-i\sigma_{yx})_1=(\sigma_{yy}-i\sigma_{yx})_2=-f'^{\infty}(x)=-(\sigma_{yy}^{\infty}-i\sigma_{yx}^{\infty})$ on L. In terms of ($\hat{\Omega}_{Sj}^{\infty}(z)$, $\hat{\Omega}_{Dj}^{\infty}(z)$), the present boundary conditions can be rewritten as:

$$\hat{\Omega}_{S1}^{\infty}(x)-\hat{\Omega}_{S2}^{\infty}(x)=0 \quad \text{on } L+L', \tag{13}$$

$$\hat{\sigma}_{D1}^{\infty}(x)+m\hat{\Omega}_{D2}^{\infty}(x)=(\hat{\Omega}_{D}^{\infty})^{+}(x)+m(\hat{\Omega}_{D}^{\infty})^{-}(x)=-\frac{(\sigma_{yy}^{\infty}-i\sigma_{yx}^{\infty})}{Q_1} \quad \text{on } L, \tag{14}$$

$$\hat{\Omega}_{D1}^{\infty}(x)-\hat{\Omega}_{D2}^{\infty}(x)=0 \quad \text{on } L', \tag{15}$$

where $m=Q_2/Q_1=(1+\beta)/(1-\beta)$. The superscripts "+" and "−" indicate the values of the quantities as they approach the interface from within the S_1 and S_2 regions, respectively. Since $\hat{\Omega}_S^{\infty}(z)$ is analytic and bounded everywhere, it must be equal to a constant by Liouville's theorem. Since the stresses vanish at infinity in this associated problem, the solution to (13) is $\hat{\Omega}_S^{\infty}(z)=0$. Note also that (14) is derived by substituting (11) and (12) into (5) and using the solution to (13).

The solution to the non-homogeneous Hilbert's problem as defined by (14) and (15) are (see Muskhelishvili, 1953):

$$\hat{\Omega}_D^{\infty}(z)=\frac{1}{2\pi i X(z)}\int_L \frac{X^{+}(x)(-f'^{\infty}(x)/Q_1)}{x-z}\,\mathrm{d}x+\frac{P^{\infty}(z)}{X(z)}, \tag{16}$$

where $1/X(z)$ is the solution to the homogeneous problem [(14) with zero on the right-hand side]. Also, $P^{\infty}(z)=C_1^{\infty}z+C_2^{\infty}$ is a polynomial of the first degree in z, since $X(z)$ has the degree 2 at infinity [see (27) below] and the stresses must vanish at infinity. Using the method described in Muskhelishvili (1953), $X(z)$ is found to be

$$X(z)=\sqrt{(z-a_1)(z-a_2)(z-a_3)(z-a_4)}\left[\frac{(z-a_2)(z-a_4)}{(z-a_1)(z-a_3)}\right]^{i\eta}, \tag{17}$$

where $\eta=\log m/(2\pi)$. Equation (17) is given in Erdogan (1965) for an arbitrary number of interfacial cracks. Expanding $X(z)$ about the point at infinity in decreasing powers of z yields:

$$X(z) = z^2 + \Delta_1 z + \Delta_2 + O\left(\frac{1}{z}\right) = h(z) + O\left(\frac{1}{z}\right), \tag{18}$$

where

$$\Delta_1 = -\frac{a_1 + a_2 + a_3 + a_4}{2} + i(a_1 + a_3 - a_2 - a_4)\eta, \tag{19}$$

$$\Delta_2 = \frac{(a_1 + a_2 + a_3 + a_4)^2 - 2(a_1^2 + a_2^2 + a_3^2 + a_4^2)}{8} - \frac{(a_1 - a_2 + a_3 - a_4)^2}{2}\eta^2 + i(a_2 a_4 - a_1 a_3)\eta. \tag{20}$$

Equation (17) is substituted into (16). Using the integration technique described in Muskhelishvili (1953), the line integral over L is replaced by a contour integral on Γ, where Γ is the union of the contours around cracks 1 and 2. Also, since $1/X(z)$ is the solution to the homogeneous Hilbert's problem, $1/X^+(x) = -m/X^-(x)$. This is made use of when Γ is shrunk onto the upper and lower faces of the cracks. The following is obtained after the above operations:

$$\begin{aligned}\hat{\Omega}_D^\infty(z) &= \frac{1}{2\pi i(1+m)X(z)}\left(\frac{-(\sigma_{yy}^\infty - i\sigma_{yx}^\infty)}{Q_1}\right)\oint_\Gamma \frac{X(x)}{x-z}\mathrm{d}x + \frac{C_1^\infty z + C_2^\infty}{X(z)}, \\ &= \frac{1}{(1+m)X(z)}\left(\frac{-(\sigma_{yy}^\infty - i\sigma_{yx}^\infty)}{Q_1}\right)[X(z) - (z^2 + \Delta_1 z + \Delta_2)] + \frac{C_1^\infty z + C_2^\infty}{X(z)}, \\ &= \frac{\sigma_{yy}^\infty - i\sigma_{yx}^\infty}{Q_1(1+m)}\left(\frac{z^2}{X(z)} - 1\right) + \frac{P_E^\infty(z)}{X(z)},\end{aligned} \tag{21}$$

where the contour integral of $X(x)/(x-z)$ around Γ equals $2\pi i(X(z) - h(z))$ and $h(z)$ is given in (18). Also, the polynomial

$$P_E^\infty(z) = E_1^\infty z + E_2^\infty \tag{22}$$

combines $P^\infty(z)$ of (16) with other terms that arise from the integrations, and for $p = 1, 2$

$$E_p^\infty = C_p^\infty + \frac{\Delta_p(\sigma_{yy}^\infty - i\sigma_{yx}^\infty)}{Q_1(1+m)}. \tag{23}$$

Converting $\hat{\Omega}_S^\infty(z) = 0$ and (21) back to the Muskhelisvili potentials by the use of (11) and (12), the following expressions are obtained:

$$\hat{\Phi}_j^\infty = \frac{m^{j-1}}{(1+m)}(\sigma_{yy}^\infty - i\sigma_{yx}^\infty)\left(\frac{z^2}{X(z)} - 1\right) + \frac{Q_j P_E^\infty(z)}{X(z)}, \tag{24}$$

$$\hat{\Psi}_j^\infty(z) = \frac{m^{k-1}}{1+m}(\sigma_{yy}^\infty + i\sigma_{yx}^\infty)\left(\frac{z^2}{\bar{X}(z)} - 1\right) + \frac{Q_k\overline{P_E^\infty}(z)}{\bar{X}(z)} - \hat{\Phi}_j^\infty(z) - z\hat{\Phi}'^\infty_j(z), \tag{25}$$

where as before $j, k \in \{1, 2\}$ but $j \neq k$. To determine the complex constants E_1^∞ and E_2^∞ of $P_E^\infty(z)$,

the uniqueness of displacement around each main crack yields two equations in the two constants. Consider the contour Γ_n, $n = 1, 2$, around each main crack. Using (7), the uniqueness of displacement around each main crack can be expressed as:

$$\oint_{\Gamma_n} \mathrm{d}(u+iv) = \oint_{\Gamma_n} \frac{\kappa_j}{2\mu_j} \hat{\Phi}_j^{\infty}(z)\,\mathrm{d}z - \oint_{\Gamma_n} \frac{1}{2\mu_j} \overline{\hat{\Psi}}_j^{\infty}(\bar{z})\,\mathrm{d}\bar{z} - \oint_{\Gamma_n} \frac{1}{2\mu_j} \mathrm{d}(z\overline{\hat{\Phi}_j^{\infty}(z)}) = 0. \tag{26}$$

Equation (26) can be replaced by line integrals in the intervals $[a_1, a_2]$ for $n = 1$ and $[a_3, a_4]$ for $n = 2$ if Γ_n is shrunk onto the crack faces. Noting that $1/X^+ = -m/X^-(x)$ and $z = \bar{z} = x$ on the crack faces, and that the upper part of Γ_n is in S_1 while the lower part of Γ_n is in S_2, (26) reduces to:

$$\frac{\sigma_{yy}^{\infty} - i\sigma_{yx}^{\infty}}{1+m} \int_{a_{2n-1}}^{a_{2n}} \frac{x^2}{X^+(x)}\,\mathrm{d}x + Q_1 \int_{a_{2n-1}}^{a_{2n}} \frac{E_1^{\infty}x + E_2^{\infty}}{X^+(x)}\,\mathrm{d}x = 0. \tag{27}$$

In deriving the above equation, the relation $(\kappa_1 - m)/2\mu_1 + (1 - m\kappa_2)/2\mu_2 = 0$ has been used. The solutions are:

$$E_p^{\infty} = (-1)^q \frac{\sigma_{yy}^{\infty} - i\sigma_{yx}^{\infty}}{(1+m)Q_1} \left(\frac{B_{22}B_{1q} - B_{12}B_{2q}}{B_{11}B_{20} - B_{21}B_{10}} \right), \tag{28}$$

where $q = p - 1$. The complex integrals B_{ns} $(s = 0, 1, 2)$ are given by:

$$B_{ns} = \int_{a_{2n-1}}^{a_{2n}} \frac{x^s}{X^+(x)}\,\mathrm{d}x. \tag{29}$$

These integrals are computed numerically by Gaussian–Jacobi quadrature. Equations (24)–(25) with (28)–(29) are the complete solutions to Associated Problem 1.

3.2. *Associated Problem* 2 *or* 3

For Problem 2 or 3, the potentials $\Phi_j^{\perp}(z)$ and $\Psi_j^{\perp}(z)$ due to an edge dislocation at z_0 in S_1 are listed in Appendix A. In Associated Problem 2 or 3 (see Fig. 1(c)), the boundary conditions are the same as (13)–(15), except that $-f^{\infty}(x) = -(\sigma_{yy}^{\infty} - i\sigma_{yx}^{\infty})$ on the right side of (14) should be replaced by the negative of the stresses due to a single dislocation, i.e.:

$$-f^{\perp}(x) = -A\left(\frac{1+\alpha}{1-\beta} \frac{1}{x - z_0} + \frac{1+\alpha}{1+\beta} \frac{1}{x - \overline{z_0}} \right) - \bar{A}\left(\frac{1+\alpha}{1+\beta} \frac{z_0 - \overline{z_0}}{(x - \overline{z_0})^2} \right), \tag{30}$$

where $A = \mu_1 \mathrm{e}^{i\theta}\{[u_r] + i[u_\theta]\}/i\pi(\kappa_1 + 1)$ characterizes the edge dislocation; e is the exponential, (r, θ) the usual polar coordinates, and $[u_r]$, $[u_\theta]$ the displacement jumps in the radial and tangential directions. Also, α and β are the Dundurs constants (see Appendix A). Equation (30) is obtained by substituting $\Phi_j^{\perp}(z)$ and $\Psi_j^{\perp}(z)$ into (5) and adding the negative sign. Note that in Fig. 1(c) $f^{\perp}(x)$ denotes the stresses due to the dislocation distribution rather than a single dislocation. The solutions to the Hilbert's problems as derived from the boundary conditions are then $\hat{\Omega}_S^{\perp}(z) = 0$ and

$$\hat{\Omega}_D^{\perp}(z) = \frac{1}{2\pi i X(z)} \int_L \frac{X^+(x)(-f^{\perp}(x)/Q_1)}{x-z} \mathrm{d}x + \frac{P^{\perp}(z)}{X(z)}, \tag{31}$$

where $P^{\perp}(z) = C_1^{\perp} z + C_2^{\perp}$, and $X(z)$ is the same as that given in (17). Substituting (30) into (31), the resulting integrals can be replaced by contour integrals in a manner similar to the replacement of (16) by (21). The contour integrals are evaluated, and the final result for $\hat{\Omega}_D^{\perp}(z)$ is:

$$\hat{\Omega}_D^{\perp}(z) = \frac{-2A}{(1+m)Q_1}\left(\frac{1+\alpha}{1-\beta}F(z,z_0) + \frac{1+\alpha}{1+\beta}F(z,\overline{z_0})\right) - \frac{2\bar{A}}{(1+m)Q_1}\left(\frac{1+\alpha}{1+\beta}(z_0-\overline{z_0})G(z,\overline{z_0})\right) + \frac{P_E^{\perp}(z)}{X(z)}, \tag{32}$$

where

$$P_E^{\perp}(z) = E_1^{\perp} z + E_2^{\perp} \tag{33}$$

combines the polynomial $P^{\perp}(z)$ of (31) with other terms that arise from the integrations, and

$$E_1^{\perp} = C_1^{\perp} + \frac{2A}{(1+m)Q_1}\frac{1+\alpha}{1-\beta^2}, \tag{34}$$

$$E_2^{\perp} = C_2^{\perp} + \frac{A}{(1+m)Q_1}\left(\frac{1+\alpha}{1-\beta}(z_0+\Delta_1) + \frac{1+\alpha}{1+\beta}(\overline{z_0}+\Delta_1)\right) + \frac{\bar{A}}{(1+m)Q_1}\left(\frac{1+\alpha}{1+\beta}(z_0-\overline{z_0})\right). \tag{35}$$

In (35), Δ_1 is given in (19). Furthermore,

$$F(z,z_0) = \frac{1}{2(z-z_0)} - \frac{1}{2(z-z_0)}\frac{X(z_0)}{X(z)}, \tag{36}$$

$$G(z,\overline{z_0}) = \frac{\partial F(z,\overline{z_0})}{\partial \overline{z_0}} = \frac{1}{2(z-\overline{z_0})^2} - \frac{1}{2(z-\overline{z_0})}\frac{X(\overline{z_0})}{X(z)}\left(\frac{1}{z-\overline{z_0}} + W(\overline{z_0})\right), \tag{37}$$

where

$$W(\overline{z_0}) = \frac{1}{2}\sum_{q=1}^{4}\frac{1}{\overline{z_0}-a_q} + i\eta\sum_{q=1}^{4}\frac{(-1)^q}{\overline{z_0}-a_q}. \tag{38}$$

Note that $W(\overline{z_0})$ arises from the differentiation of $X(\overline{z_0})$, i.e. $\mathrm{d}[X(\overline{z_0})]/\mathrm{d}\overline{z_0} = W(\overline{z_0})X(\overline{z_0})$.

Converting $\hat{\Omega}_S^{\perp}(z) = 0$ and (32) back to the Muskhelishvili potentials by the use of (11) and (12), the following expressions are obtained:

$$\hat{\Phi}_1^{\perp}(z) = \frac{-2A}{1+m}\left(\frac{1+\alpha}{1-\beta}F(z,z_0)+\frac{1+\alpha}{1+\beta}F(z,\overline{z_0})\right)-\frac{2\bar{A}}{1+m}\frac{1+\alpha}{1+\beta}(z_0-\overline{z_0})G(z,\overline{z_0})+Q_1\frac{P_E^{\perp}(z)}{X(z)}, \tag{39}$$

$$\hat{\Psi}_1^{\perp}(z)+\frac{\mathrm{d}}{\mathrm{d}z}(z\hat{\Phi}_1^{\perp}(z)) = \frac{-2m\bar{A}}{1+m}\left(\frac{1+\alpha}{1-\beta}\overline{F(\bar{z},z_0)}+\frac{1+\alpha}{1+\beta}\overline{F(\bar{z},\overline{z_0})}\right) - \frac{2mA}{1+m}\frac{1+\alpha}{1+\beta}(\overline{z_0}-z_0)\overline{G(\bar{z},\overline{z_0})}+Q_2\frac{\overline{P_E^{\perp}(\bar{z})}}{\overline{X(\bar{z})}}, \tag{40}$$

$$\hat{\Phi}_2^{\perp}(z) = m\hat{\Phi}_1^{\perp}(z), \tag{41}$$

$$\hat{\Psi}_2^{\perp}(z)+\frac{\mathrm{d}}{\mathrm{d}z}(z\hat{\Phi}_2^{\perp}(z)) = \frac{1}{m}\left[\hat{\Psi}_1^{\perp}(z)+\frac{\mathrm{d}}{\mathrm{d}z}(z\hat{\Phi}_1^{\perp}(z))\right]. \tag{42}$$

Two sets of complex constants $E_1^{\perp}$ and $E_2^{\perp}$ can be determined for $P_E^{\perp}(z)$. The first set $(E_1^{\perp 1}, E_2^{\perp 1})$ corresponds to the location of z_0 on the kink associated with crack 1 (Problem 2), while the second set $(E_1^{\perp 2}, E_2^{\perp 2})$ to the location of z_0 on the kink associated with crack 2 (Problem 3). As in (26), $\mathrm{d}(u+iv)$ is integrated around two contours, resulting in two equations.

To determine $(E_1^{\perp 1}, E_2^{\perp 1})$, the contour Γ_1 encloses main crack 1 and the trace of the associated kink, including the dislocation at z_0 on the trace, while the contour Γ_2 encloses main crack 2 only. Taking steps similar to those leading to (27), Γ_1 is shrunk onto the faces of main crack 1 and the associated kink, while Γ_2 is shrunk onto the faces of main crack 2. The integration around the trace of the kink is zero since all the integrands are analytic on the kink including at z_0. If the integrations stated in (26) are carried out using the potentials of (39)–(42), the following is obtained:

$$\begin{aligned}
&\frac{A}{mQ_1}\left[\frac{1+\alpha}{1-\beta}X(z_0)\int_{a_{2n-1}}^{a_{2n}}\frac{1}{X^+(x)(x-z_0)}\mathrm{d}x+\frac{1+\alpha}{1+\beta}X(\overline{z_0})\right.\\
&\left.\times\int_{a_{2n-1}}^{a_{2n}}\frac{1}{X^+(x)(x-\overline{z_0})}\mathrm{d}x\right]+\frac{\bar{A}}{mQ_1}\frac{1+\alpha}{1+\beta}(z_0-\overline{z_0})X(\overline{z_0})\left[\int_{a_{2n-1}}^{a_{2n}}\frac{1}{X^+(x)(x-\overline{z_0})^2}\mathrm{d}x\right.\\
&\left.+W(\overline{z_0})\int_{a_{2n-1}}^{a_{2n}}\frac{1}{X^+(x)(x-\overline{z_0})}\mathrm{d}x\right]+\frac{1+m}{m}\left(E_1^{\perp 1}\int_{a_{2n-1}}^{a_{2n}}\frac{x}{X^+(x)}\mathrm{d}x+E_2^{\perp 1}\int_{a_{2n-1}}^{a_{2n}}\frac{1}{X^+(x)}\mathrm{d}x\right)\\
&=\begin{cases}A\pi i(\kappa_1+1)\mu_1 & \text{for } n=1,\\ 0 & \text{for } n=2,\end{cases}
\end{aligned} \tag{43}$$

where $n=1$, 2 identifies the contour Γ_n, and $A\pi i(\kappa_1+1)/\mu_1 = \mathrm{e}^{i\theta}$ $([u_r]+i[u_\theta])$ is the dislocation content within Γ_1. To determine $E_1^{\perp 2}$, $E_2^{\perp 2}$, an equation similar to (43) can be obtained, with the difference that Γ_1 encloses main crack 1 and has no net dislocation content whereas Γ_2 encloses main crack 2 and the dislocation at z_0 on the trace of the associated kink. Defining $N = n+(-1)^{n+1}$ and recalling that $q = p-1$, the explicit forms for the two sets of parameters are:

$$E_p^{\perp n} = \frac{(-1)^q}{B_{11}B_{20}-B_{10}B_{21}}\Bigg[(-1)^{n+1}\frac{m}{1+m}\frac{A\pi i(\kappa_1+1)}{\mu_1}B_{Nq}$$
$$+\frac{A}{(1+m)Q_1}\frac{1+\alpha}{1-\beta}[B_{1q}D_{21}(z_0)-B_{2q}D_{11}(z_0)]X(z_0)$$
$$+\frac{A}{(1+m)Q_1}\frac{1+\alpha}{1+\beta}[B_{1q}D_{21}(\overline{z_0})-B_{2q}D_{11}(\overline{z_0})]X(\overline{z_0})$$
$$+\frac{\bar{A}}{(1+m)Q_1}\frac{1+\alpha}{1+\beta}[B_{1q}D_{22}(\overline{z_0})-B_{2q}D_{12}(\overline{z_0})](z_0-\overline{z_0})X(\overline{z_0})$$
$$+\frac{\bar{A}}{(1+m)Q_1}\frac{1+\alpha}{1+\beta}[B_{1q}D_{21}(\overline{z_0})-B_{2q}D_{11}(\overline{z_0})](z_0-\overline{z_0})X(\overline{z_0})W(\overline{z_0})\Bigg], \tag{44}$$

where the complex integrals

$$D_{ns}(z_0) = \int_{a_{2n-1}}^{a_{2n}} \frac{1}{X^+(x)(x-z_0)^s}\,\mathrm{d}x \tag{45}$$

are evaluated numerically for $s = 1, 2$ by Gaussian–Jacobi quadrature. The integrals B_{ns} are given in (29). Equations (39)–(42) with (44)–(45) are the complete solutions to Associated Problem 2 or 3. Equations (30)–(45) have been derived on the assumption that $z_0 \in S_1$. When $z_0 \in S_2$, it is only necessary to replace (α, β) by $(-\alpha, -\beta)$ in these equations, and to replace $A\pi i(\kappa_1+1)/\mu_1$ in (43)–(44) by $A\pi i(\kappa_2+1)/\mu_2$. The exception is that the sign of β in $m = (1+\beta)/(1-\beta)$ is not changed.

For a distribution of dislocations, A is interpreted as a dislocation density and the corresponding solutions can be obtained by integrating the solutions for a single dislocation over the positions occupied by the dislocation group.

4. Integral equations, stress intensity factors and energy release rate

To satisfy (4), the normal and shear stresses at the kink locations in all problems are superimposed and set equal to zero. Figure 1 can be used as an example, in which a kink is joined to the inner tip of each interfacial crack. Let z_1 and z_2 denote the positions along kinks 1 and 2, respectively, and similarly z_{01} and z_{02} the positions of the dislocations on kinks 1 and 2. If t denotes the position along either kink with origin at the kink knee, then the superimposition of the stresses results in the following two complex, or four real, integral equations for $n = 1, 2$:

$$\int_0^{l_1}[\sigma_{\theta\theta}^{\perp}(z_n, z_{01}) + i\sigma_{r\theta}^{\perp}(z_n, z_{01}) + \hat{\sigma}_{\theta\theta}^{\perp}(z_n, z_{01}) + i\hat{\sigma}_{r\theta}^{\perp}(z_n, z_{01})]\,\mathrm{d}t$$
$$+\int_0^{l_2}[\sigma_{\theta\theta}^{\perp}(z_n, z_{02}) + i\sigma_{r\theta}^{\perp}(z_n, z_{02}) + \hat{\sigma}_{\theta\theta}^{\perp}(z_n, z_{02}) + i\hat{\sigma}_{r\theta}^{\perp}(z_n, z_{02})]\,\mathrm{d}t$$
$$+[\sigma_{\theta\theta}^{\infty}(z_n) + i\sigma_{r\theta}^{\infty}(z_n) + \hat{\sigma}_{\theta\theta}^{\infty}(z_n) + i\hat{\sigma}_{r\theta}^{\infty}(z_n)] = 0. \tag{46}$$

The superscripts on the stress components indicate the potential functions from which they should be computed. The three sets of rectangular brackets correspond to Problems 2, 3 and 1, respectively. The last two terms within each set of brackets correspond to the associated problem. It can be easily verified that the equations are of the singular Cauchy type and the two unknown functions are the dislocation densities in kinks 1 and 2, i.e. A_n, $n = 1, 2$.

Equation (46) is solved by the method of piecewise polynomials (Gerasoulis, 1982). The method has been used for solving kinked crack problems (He and Hutchinson, 1989; Obata et al., 1989; Mukai et al., 1990; Niu and Wu, 1997). Essentially, each dislocation density $A_n(t')$ is written as the product of a weight function $w(t')$ and a regular function $\varphi_n(t')$, where $t'(-1 \leqslant t' \leqslant 1)$ describes the normalized position along either kink. The values $t' = 1$ and $t' = -1$ denote positions at the kink tip and the kink knee, respectively. Additional conditions $\varphi_n(-1) = 0$ are used to solve the problem. Dividing the normalized interval $[-1, 1]$ into R intervals, the use of R collocation points within the intervals generates R linear algebraic equations for each integral equation. Together with the additional conditions, a system of $4(R+1)$ linear algebraic equations is obtained with $\varphi_n(t')$ at the boundary points of the R intervals as unknowns.

After solving the algebraic equations, the mode I and mode II SIFs (K_{I}, K_{II}) of kink n are easily calculated from the stress field around the kink tip. The formula is (see also Lo, 1978):

$$K_{\mathrm{I}} + iK_{\mathrm{II}} = (\pi)^{3/2}(2l)^{1/2}\, \mathrm{e}^{i\theta_n}\overline{\varphi_n(1)}, \tag{47}$$

where θ_n is the orientation of the kink. The energy release rate under the plane strain condition is given by the classical formula

$$G = \frac{1+\kappa_j}{8\mu_j}(K_{\mathrm{I}}^2 + K_{\mathrm{II}}^2). \tag{48}$$

To compare the numerical results with previously published results, (48) is normalized by the energy release rate G_0 at the tip of an equivalent straight interfacial crack of total length $2c' = 2c + l$. The expression for G_0 is (see, e.g. Malyshev and Salganik, 1965):

$$G_0 = \left(\frac{1+\kappa_1}{8\mu_1} + \frac{1+\kappa_2}{8\mu_2}\right)\frac{(1+4\eta^2)[(\sigma_{yy}^{\infty})^2 + (\sigma_{yx}^{\infty})^2]\pi c'}{2\cosh^2(\pi\eta)}. \tag{49}$$

5. Numerical results

A remote tensile stress σ is applied in the direction perpendicular to the main cracks. More complicated loadings involving remote shear and tension are not considered; the objective is to show that even under remote tension complex phenomena exist due to crack interactions.

The geometrical parameters $2c$, l and $2d$ denote, respectively, the length of the main crack, the length of the kink, and the distance between the inner tips of the main cracks. A distance parameter $\delta = (d-l)/(2c+d)$ is used to characterize the interaction. Unless otherwise stated, the two cracks are arranged symmetrically about the y-axis. When the cracks are unequal, subscripts are used to distinguish between them, e.g. $2c_1$, $2c_2$, etc.

All numerical integrations are performed with the 50-point Gaussian–Jacobi quadrature

Table 1.
Stress intensity factors, $\tilde{K}_{\mathrm{I}} = K_{\mathrm{I}}/\sigma_{yy}^{\infty}\sqrt{\pi(c+l/2)}$, of two interacting straight cracks in a homogeneous material with no interface. The approximate solutions are obtained by treating the light parts of the straight cracks as dislocation distributions. The solutions improve with an increase in R, i.e. the number of collocation points used to solve the governing integral equations

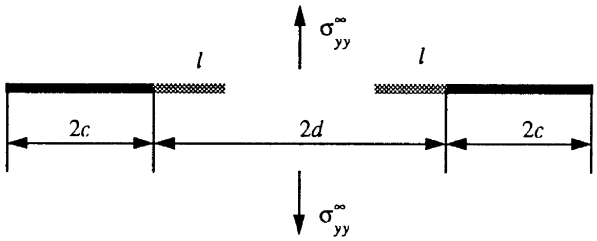

$\delta = [(d-l)/(2c+d)]$	Exact solutions Erdogan (1962)	$c/l = 1$			$c/l = 100$		
		$R = 16$	$R = 64$	$R = 128$	$R = 16$	$R = 64$	$R = 128$
0.0001	13.347	5.315	8.592	10.368	13.080	13.300	13.318
0.001	5.395	4.375	5.204	5.331	5.367	5.382	5.384
0.01	2.372	2.349	2.370	2.371	2.362	2.367	2.368
0.02	1.905	1.898	1.904	1.904	1.897	1.901	1.902
0.05	1.473	1.471	1.472	1.473	1.467	1.471	1.471
0.1	1.255	1.254	1.255	1.255	1.250	1.253	1.254
0.2	1.112	1.111	1.112	1.112	1.108	1.111	1.111
0.99	1.000	0.999	1.000	1.000	0.996	0.999	0.999

formula. All solutions of the integral equations, except for some results in Section 5.1.1 below, are generated with R in the range $64 \leqslant R \leqslant 240$.

5.1. *Test cases*

5.1.1. *Two interacting straight cracks in an isotropic homogeneous solid*

The SIF solutions for two identical straight cracks each joined by a "kink" of 0 or 180° angle in an isotropic homogeneous solid are compared to the exact solutions of Erdogan (1962). The comparison is shown in Table 1, which contains three sets of normalized K_{I} solutions for various crack separations: (i) the exact solutions obtained by treating each crack as an uninterrupted straight crack, (ii) the approximate solutions obtained by treating each crack as a main crack joined by a kink with $c/l = 1$, and (iii) the approximate solutions obtained as in (ii) but with $c/l = 100$. The approximate solutions, obtained using $\kappa_1 = \kappa_2$, $\mu_1 = \mu_2$ and $R = 16$, 64, 128, agree well with the exact solutions. The errors are less than 1% when δ is greater than or equal to 0.01. For $\delta = 0.001$ and 0.0001, the approximate solutions tend towards the exact solutions of 5.395 and 13.347 (in three decimal places) as R increases. The best approximate solution of 13.318 for $\delta = 0.0001$, computed using $c/l = 100$ and $R = 128$, represents an error of approximately 0.2%.

The comparison shows that the kinked interfacial crack model, when specialized for the case of strongly interacting straight cracks in an isotropic homogeneous solid, produces accurate SIFs. The accuracy is excellent provided R is sufficiently large. When the kink angles are not zero, the current model predictions agree with the results of Lo (1978) for a single kinked crack and also those of Niu and Wu (1997) for two strongly interacting kinked cracks.

5.1.2. *Two kinked interfacial cracks located at a large distance from each other*
When there exists an interface separating two materials, the current results agree with those presented in Mukai et al. (1990) for a single kinked interfacial crack. An example is provided here in which two identical kinked cracks are separated by a very large distance ($\delta = 1$–10^{-9}). Figure 2 plots the normalized energy release rate $\tilde{G} = G/G_0$ vs the kink angle θ for $l/c = 0.001$ and various values of α, β. Also plotted is $\tilde{G}$ vs θ for $\alpha = 0.5$, $\beta = 0.14286$ and $l/c = 0.001$, 0.01, 0.1, 1. The symbols in the figure indicate the results of Mukai et al. (1990), while the full lines indicate the current model predictions. The two sets of results agree well.

5.2. *Symmetric configuration*

Consider two identical kinked interfacial cracks located symmetrically about the y-axis. The kinks are infinitesimally small compared to the main cracks. The parameters used are $\mu_{21} = \mu_2/\mu_1 = 3$, 100, $v_1 = v_2 = 0.3$. These correspond to $(\alpha, \beta) = 0.5$, 0.14286 and $(\alpha, \beta) = 0.98020$, 0.28006, respectively. Also, $l/c = 0.001$ and $\delta = 0.99$, 0.1, 0.01, 0.001, 0.0001. Since $\mu_2 > \mu_1$, S_2 and S_1 are for convenience called "stiff" and "compliant" materials. The SIFs are normalized, i.e. $\tilde{K}_{\mathrm{I}} = K_{\mathrm{I}}/\sigma_{yy}^{\infty}\sqrt{\pi c'}$, $\tilde{K}_{\mathrm{II}} = K_{\mathrm{II}}/\sigma_{yy}^{\infty}\sqrt{\pi c'}$. Due to symmetry, it is sufficient to plot the SIFs and the energy release rate of kink 1. The mode mixity is defined as $\gamma = \tan^{-1}(K_{\mathrm{II}}/K_{\mathrm{I}})$. Results for kinks almost parallel to the interface are omitted due to numerical inaccuracies.

5.2.1. *Effect of interaction on SIFs, energy release rate, mode mixity and critical kink angle*
Figure 3 plots $\tilde{K}_{\mathrm{I}}$, $\tilde{K}_{\mathrm{II}}$ and $\tilde{G}$ vs the kink angle θ for $\mu_{21} = 3$. As expected, they generally increase in magnitude as δ decreases. Local maxima of the $\tilde{K}_{\mathrm{I}}$–θ curves exist for positive θ, i.e. in the compliant material S_1. These local $\tilde{K}_{\mathrm{I}}$ maxima are, however, less than the maximum values of $\tilde{K}_{\mathrm{I}}$ in the stiff material S_2. In contrast, the $\tilde{G}$ values in S_1, which also display maxima, are greater than the maximum $\tilde{G}$ values in S_2. The $\tilde{K}_{\mathrm{II}}$–θ curves possess zeroes in S_1. Assuming for the time being that the cracks kink into the compliant material, then the critical kink angle θ_{cr}, whether predicted by the local maximum K_{I} criterion, the maximum G criterion or the $K_{\mathrm{II}} = 0$ criterion, decreases with increase in $1/\delta$. Figure 4 shows that as $1/\delta$ increases through four orders of magnitude, θ_{cr} decreases from ~ 35–$\sim 10^{\circ}$ for $\mu_{21} = 3$, and from ~ 55–$\sim 15^{\circ}$ for $\mu_{21} = 100$. Furthermore, the variations of the mode mixity γ with θ and δ are also shown in Fig. 5 for $\mu_{21} = 3$. If the kinks are in S_1 and the interaction increases at a given kink angle, the mode mixity increases towards mode I ($\gamma = 0^{\circ}$) if the kink angle is small ($< \sim 30^{\circ}$), but increases towards node II ($\gamma = 90^{\circ}$) if the kink angle is large ($> \sim 30^{\circ}$). When the kinks are in S_2, an increase in interaction leads to the increase of the mode mixity towards mode I.

The first implication is that interaction between the interfacial cracks reduces the critical kink angle. This result is intuitive since the attraction between the interfacial crack reduces the tendency to kink out of plane. The tendency to kink, however, is stronger than the tendency for the interfacial

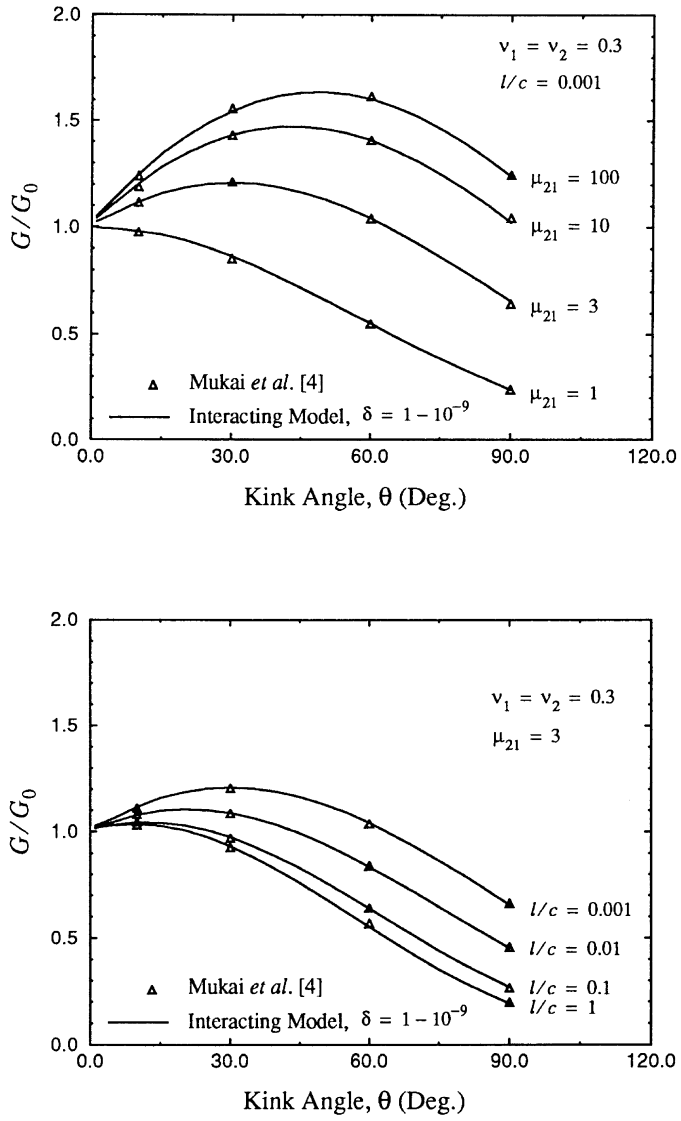

Fig. 2. Comparison of the energy release rates computed using a single crack model and a crack interaction model.

cracks to join each other along the interface, since finite critical kink angles are predicted even when the interfacial crack tips are separated by a distance as small as $2d = 0.0024c$ ($\delta = 0.0001$). The second implication is that the critical kink angle predictions of all three criteria agree to within ten degrees and interaction does not cause significant differences between the predictions. Finally, the interaction may have opposite effects on the mode mixity in the compliant and stiff materials. It increases the mode I mixity in the stiff material, but reduced it in the compliant material if the kink angle is sufficiently large.

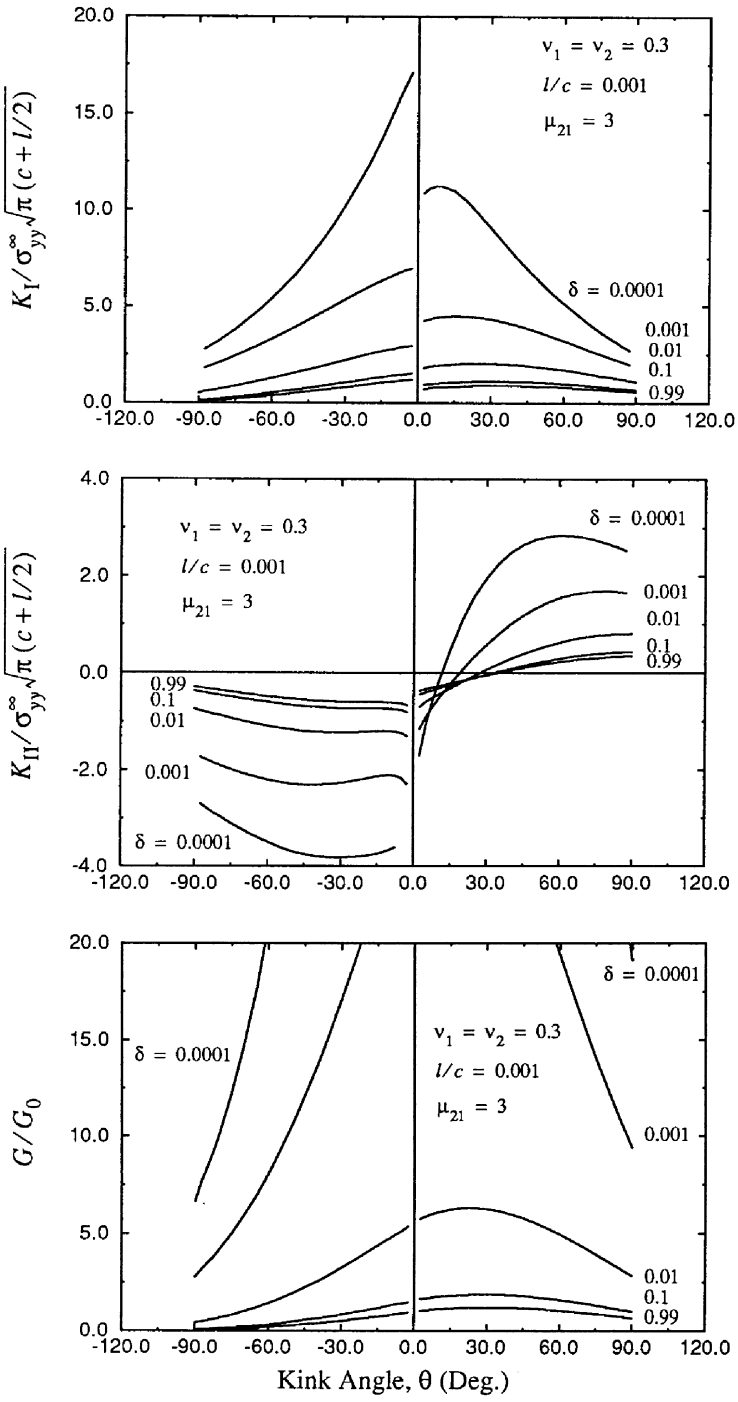

Fig. 3. Dependence of the SIFs and the energy release rate on the distance parameter δ of two kinked interfacial cracks which are symmetric about the y-axis.

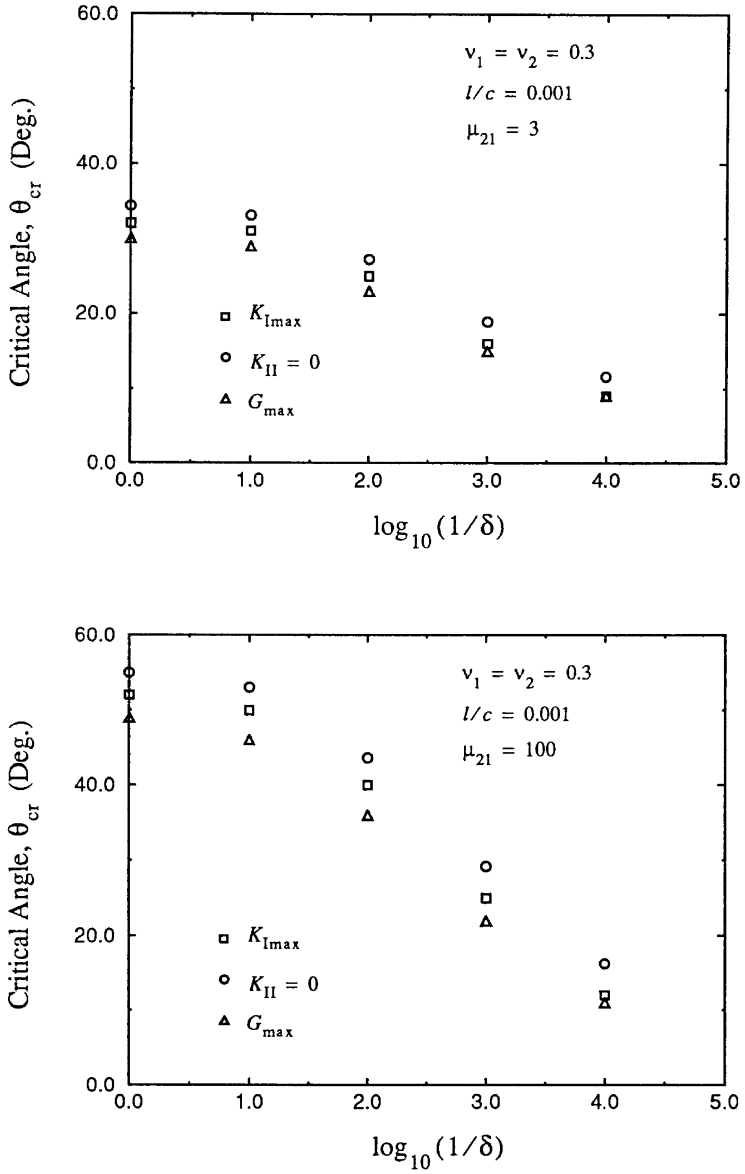

Fig. 4. Decrease of the critical angle with increase in interaction strength, assuming that kinking occurs in the compliant material.

5.2.2. *Consideration of fracture toughness*

It is necessary to consider the fracture toughness of both materials and the interface. Since the materials are isotropic, the critical energy release rate, G_C, is related to the critical mode I SIF, K_{IC} (plane strain fracture toughness), by $G_C = K_{IC}^2(1-v^2)/E$ for each material, where E and v are,

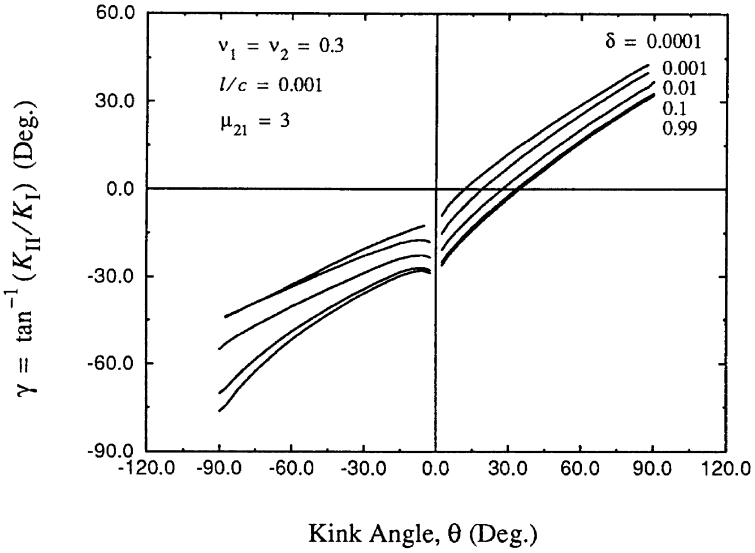

Fig. 5. Influence of the interaction strength on the mode mixity of a kink in the two parts of the bi-material.

respectively, the Young's modulus and the Poisson's ratio. Kinking into S_1 is unlikely to occur compared to kinking into S_2 or interfacial fracture if the following equation is satisfied:

$$\frac{K_{\mathrm{Imax},2}}{K_{\mathrm{Imax},1}} > \frac{K_{\mathrm{IC},2}}{K_{\mathrm{IC},1}}, \quad \text{or} \quad \frac{G_{\mathrm{max},2}}{G_{\mathrm{max},1}} > \frac{G_{\mathrm{C},2}}{G_{\mathrm{C},1}}, \tag{50}$$

where $K_{\mathrm{Imax},2}/K_{\mathrm{Imax},1}$ and $K_{\mathrm{IC},2}/K_{\mathrm{IC},1}$ denote, respectively, the ratio of the maximum mode I SIFs and the ratio of the plane strain fracture toughnesses of the two materials, and the ratios $G_{\mathrm{max},2}/G_{\mathrm{max},1}$ and $G_{\mathrm{C},2}/G_{\mathrm{C},1}$ are similarly defined. To simplify the discussion, it is assumed that the interface is at least as tough as the less tough material.

The maximum K_I criterion has been regarded as a possible method for predicting the fracture angles of interfacial cracks (Miller and Stock, 1989). So has the maximum G criterion (He and Hutchinson, 1989). It is useful to compare the predictions of both criteria and to investigate if interaction can lead to discrepancies in the predictions. For this purpose consider the case of $K_{\mathrm{IC},2}/K_{\mathrm{IC},1} = 100$ MPa $\mathrm{m}^{1/2}/70$ MPa $\mathrm{m}^{1/2} = 1.43$ and $\mu_{21} = 80.7$ GPa/26.9 GPa $= 3$ (e.g. an aluminum–nickel or aluminum–steel bi-material). Assuming that the Poisson's ratios of the metals are 0.3, the corresponding ratio $G_{\mathrm{C},2}/G_{\mathrm{C},1} = 43.3\ \mathrm{kJm}^{-2}/63.7\ \mathrm{kJm}^{-2} = 0.68$.

Making use of Fig. 3 in which $\mu_{21} = 3$, Fig. 6 plots $K_{\mathrm{Imax},2}/K_{\mathrm{Imax},1}$ and $G_{\mathrm{max},2}/G_{\mathrm{max},1}$ as a function of $\log_{10}(1/\delta)$. The values of $K_{1\mathrm{max},2}$ and $G_{\mathrm{max},2}$ are estimated from the values at $\theta \sim 0^\circ$. It can be seen that $1.35 < K_{\mathrm{Imax},2}/K_{\mathrm{Imax},1} < 1.55$ due to interaction. If $K_{\mathrm{IC},2}/K_{\mathrm{IC},1}$ falls within the range of $K_{\mathrm{Imax},2}/K_{\mathrm{Imax},1}$, whether the crack extends by kinking into S_1 or S_2 or by self-similar growth depends on the interaction strength. In the present case of $K_{\mathrm{IC},2}/K_{\mathrm{IC},1} = 1.43$, $K_{\mathrm{Imax},2}/K_{\mathrm{Imax},1}$ is smaller than $K_{\mathrm{IC},2}/K_{\mathrm{IC},1}$ for $\log_{10}(1/\delta) < \sim 1.25$ but larger than $K_{\mathrm{IC},2}/K_{\mathrm{IC},1}$ for $\log_{10}(1/\delta) > \sim 1.25$. Thus, according to the maximum K_I criterion weakly interacting cracks may kink into the compliant material whereas strongly interacting cracks may either extend self-similarly or kink into the stiff

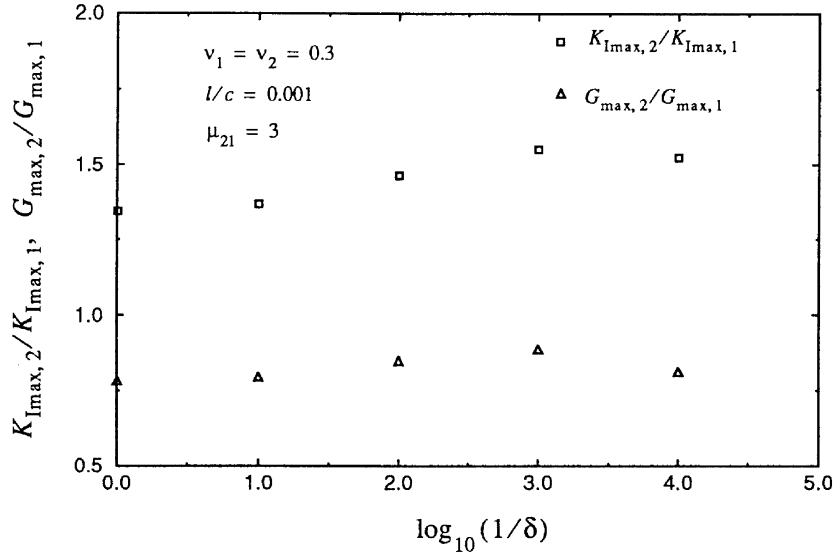

Fig. 6. Variation of the ratio of the maximum mode I SIFs and the ratio of the maximum energy release rates in the two materials with the interaction strength.

material instead. Since $\tilde{K}_{\mathrm{I}}$ appears to reach its maximum in S_2 at the interface in the case of $\mu_{21} = 3$, self-similar extension rather than kinking into S_2 is likely. The latter scenario may be possible, however, if μ_{21} assumes another value, since further results (not included here) indicate that $\tilde{K}_{\mathrm{I}}$ reaches its maximum at some non-zero angle in S_2 if $\mu_{21} = 100$.

Contrary to the results of Fig. 4, the maximum G and maximum K_{I} criteria to not always agree closely in the prediction of θ_{cr}. In the example above, $0.75 < G_{\mathrm{max},2}/G_{\mathrm{max},1} < 0.85$ due to interaction (see Fig. 6). The ratio $G_{\mathrm{C},2}/G_{\mathrm{C},1} = 0.68$ is, however, always smaller than $G_{\mathrm{max},2}/G_{\mathrm{max},1}$. Since $G_{\mathrm{max},2}$ occurs at $\theta = 0^\circ$, the interfacial cracks tend to extend self-similarly irrespective of the interaction strength. In other words, the maximum G criterion predicts $\theta_{\mathrm{cr}} = 0^\circ$ regardless of interaction, while the maximum K_{I} criterion predicts $\theta_{\mathrm{cr}} \sim 32^\circ$ for weakly interacting cracks but $\theta_{\mathrm{cr}} = 0^\circ$ for strongly interacting cracks. The upper plot of Fig. 7 summarizes the above discussion by plotting θ_{cr} as predicted by the two criteria against $\log_{10}(1/\delta)$. It is noted that even though the combination of $G_{\mathrm{max},1} > G_{\mathrm{max},2}$ and $K_{\mathrm{IC},2} > K_{\mathrm{IC},1}$ encourages kinking into the compliant material, this does not occur according to the maximum G criterion since the smaller shear modulus of the compliant material results in $G_{\mathrm{C},1} > G_{\mathrm{C},2}$.

The lower plot of Fig. 7 compares the critical remote "stresses" (containing the factor $\sqrt{\pi c'}$) as predicted by the two criteria. The maximum G criterion is satisfied at a lower critical stress than the maximum K_{I} criterion, whether the discrepancies in θ_{cr} are large or small. Further work substantiated by experimental investigation, however, is necessary to answer the question as to which of the two predictions is correct.

In general, the relevant parameters affecting the kinking behavior are many and may have significant variability. For instance, the ranges of $K_{\mathrm{Imax},2}/K_{\mathrm{Imax},1}$ and $G_{\mathrm{max},2}/G_{\mathrm{max},1}$ depend on the Dundurs parameters and the crack configuration, and there can be significant variability of K_{IC} or G_{C} due to differences in material microstructure (alloying elements, impurities) or material types

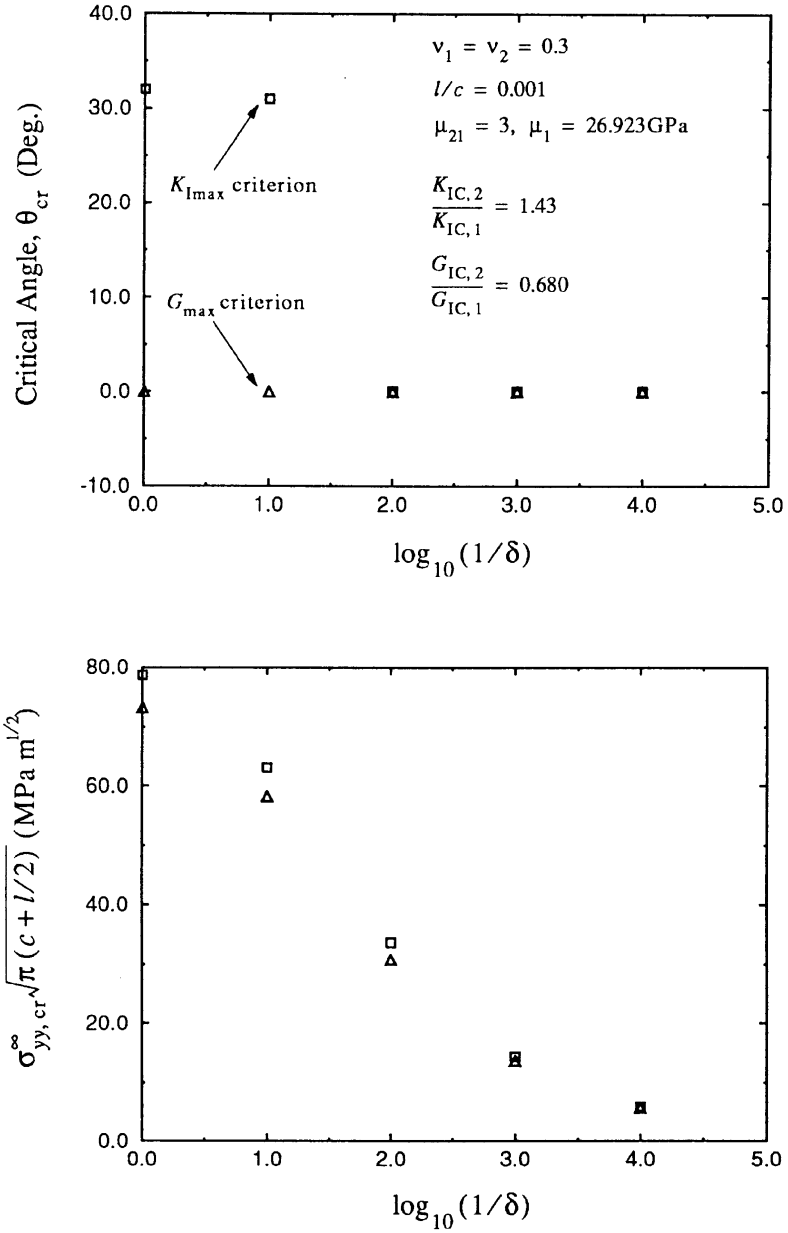

Fig. 7. Effect of interaction on the critical angle and the critical stress predictions, and discrepancies between the maximum K_I criterion and the maximum G criterion. The crack configuration is symmetric.

(metal–ceramic or other bi-materials). Considering the differences in material microstructure, the range of K_{IC} for steel can be 50–170 MPa m$^{1/2}$. For aluminum the range can be 10–70 MPa m$^{1/2}$. Thus, $K_{IC,2}/K_{IC,1}$ lies between 0.72 and 17, while $G_{C,2}/G_{C,1}$ lies between 0.17 and 96.3. For the ranges of $K_{Imax,2}/K_{Imax,1}$ and $G_{max,2}/G_{max,1}$ predicted, there will be material combinations such that kinking

always occurs in the stiff or compliant material regardless of the interaction, or kinking may occur in the stiff or compliant material depending on the interaction.

5.3. *Asymmetric configuration*

Consider two unequal kinked interfacial cracks located on either side of the y-axis. The parameters considered are $\mu_{21} = \mu_2/\mu_1 = 3, 100$, $v_1 = v_2 = 0.3$, and $\delta = 0.99, 0.01, 0.001$.

5.3.1. *Unequal main cracks with equal kinks*

The effect of unequal main cracks on equal kinks is examined. For this purpose, choose $c_1/c_2 = 5$, and $l_1/c_2 = l_2/c_2 = 0.001$. The main crack on the left (crack 1) is five times longer than the one on the right (crack 2), although the kink lengths are the same. The kink angles satisfy the relation $\theta_1 + \theta_2 = 180^\circ$, and the variable $\theta = \theta_1$ is used in the figures. Figure 8 plots $\tilde{K}_\mathrm{I}$, $\tilde{K}_\mathrm{II}$ and $\tilde{G}$ vs θ for the case of $\mu_{21} = 100$ and $\delta = (d - l_2)/(2c_2 + d) = 0.99, 0.01$. The factor of non-dimensionalization for the SIFs is $\sigma^{\infty}_{yy}\sqrt{\pi c'_2}$. For G it is G_{02}, given by (49) with $c' = c'_2$.

In the compliant material, $\tilde{K}_\mathrm{I}$ and $\tilde{G}$ of kink 1 are generally greater than those of kink 2 for $\delta = 0.99$ and 0.01. In the stiff material, although $\tilde{K}_1$ and $\tilde{G}$ of kink 1 are greater than those of kink 2 for $\delta = 0.99$, they are smaller for $\delta = 0.01$. This represents an anomalous effect due to interaction, and may have the following consequence. Suppose that (50) is satisfied whether the maximum K_I or the maximum G criterion is used, i.e. kinking into the compliant material S_1 is not likely. In the case of very weak interaction, both criteria will then predict that kink extension from the long main crack will occur parallel to the interface before a similar extension can occur from the short main crack. The reverse occurs in the case of strong interaction, i.e. the short main crack will extend first, contrary to intuition. The discussion here, however, is subjected to the restriction that $\theta_1 + \theta_2 = 180^\circ$. A definite conclusion is possible only if a comprehensive search is carried out for the combination of θ_1 and θ_2 that yields the maximum $\tilde{K}_\mathrm{I}$ or $\tilde{G}$.

5.3.2. *Equal main cracks with unequal kinks*

The extension of an infinitesimal kink in the presence of a finite kink is examined. For this purpose, choose $c_1/c_2 = 1$, $l_1/c_2 = 0.001$, and $l_2/c_2 = 0.1$. Kink 1 is a hundred times shorter than kink 2. Also, $\theta_2 = 150^\circ$ while θ_1 is allowed to vary between -90 and 90°. Figure 9 plots $\tilde{K}_\mathrm{I}$, $\tilde{K}_\mathrm{II}$ and $\tilde{G}$ vs θ_1 for the case of $\mu_{21} = 3$ and $\delta = (d - l_1)/(2c_1 + d) = 0.99, 0.01, 0.001$. Unlike Fig. 8, the non-dimensionalization factors consist of the length c'_1.

In contrast to the previous results, the interaction of the finite and infinitesimal kinks causes complex shielding of the SIFs and the energy release rates. As δ decreases from 0.99–0.001, the finite kink first experiences an increase in $\tilde{K}_\mathrm{I}$ and $\tilde{G}$ but subsequently a considerable decrease of these parameters at $\delta = 0.001$. This implies that the shielding due to the finite kink dominates over the amplification associated with a decrease in δ. Also, although the angle of the finite kink is held fixed, $\tilde{K}_\mathrm{I}$, $\tilde{K}_\mathrm{II}$ and $\tilde{G}$ of the finite kink all experience jumps in various degrees as the infinitesimal kink crosses the material interface.

Consider next the infinitesimal kink. It is interesting to observe that the shielding of $\tilde{K}_\mathrm{I}$ and $\tilde{G}$ of the infinitesimal kink is less than that of the considerably longer finite kink for almost all θ_1. Furthermore, the $\tilde{K}_\mathrm{I}$ and $\tilde{G}$ curves for the various values of δ may intersect each other. The maximum values of $\tilde{K}_\mathrm{I}$ and $\tilde{G}$ for $\delta = 0.001$ are smaller than the corresponding maximum values

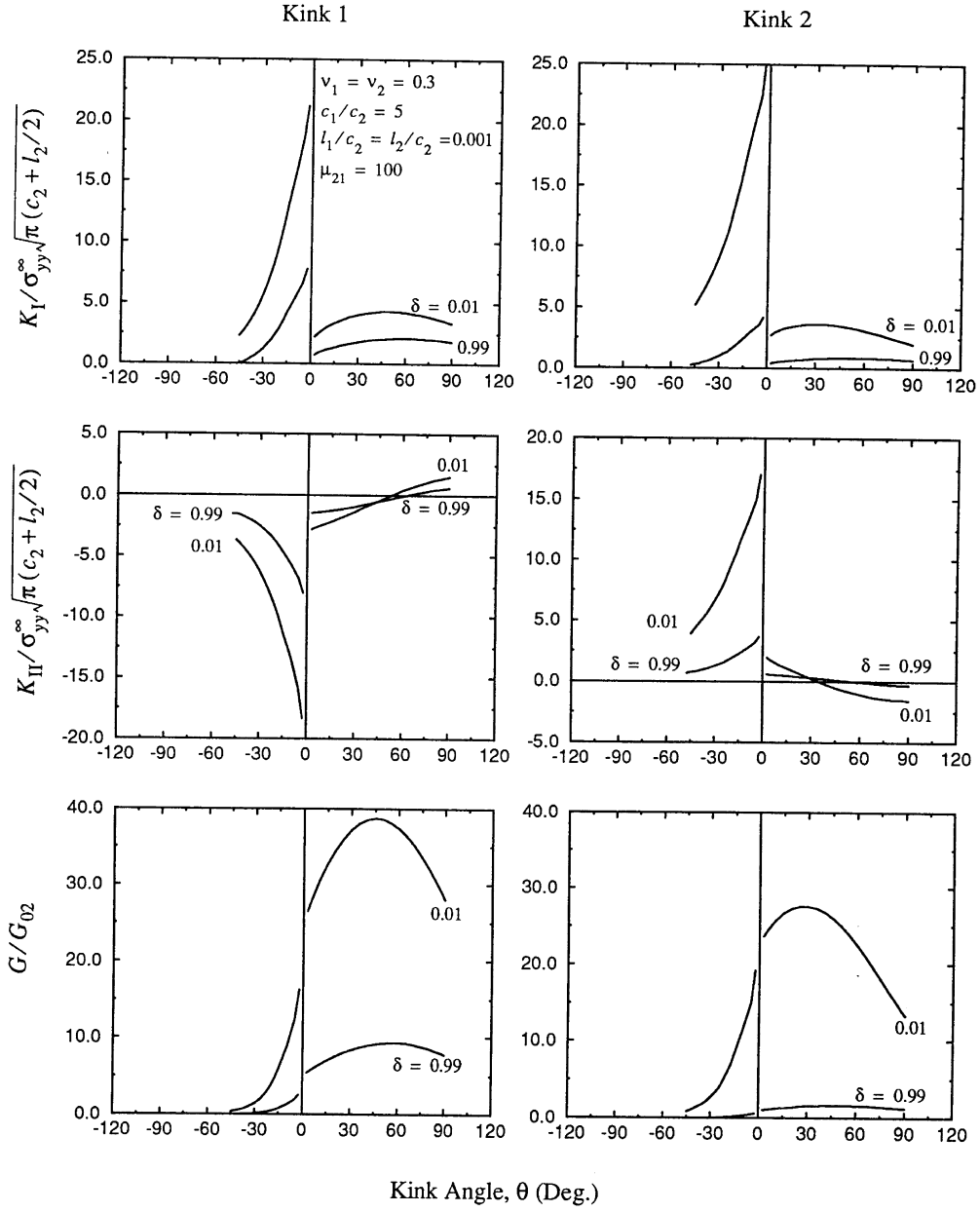

Fig. 8. Dependence of the SIFs and the energy release rate on the distance parameter δ of two kinked interfacial cracks containing unequal interfacial parts and equal kinks.

for $\delta = 0.01$, whether the infinitesimal kink is in S_1 or S_2. Also, the maxima of $\tilde{K}_I$ and $\tilde{G}$ in S_1 occur at increasingly larger θ_1 as δ decreases. These anomalies are not present in the symmetric case or in the asymmetric case of Section 5.3.1.

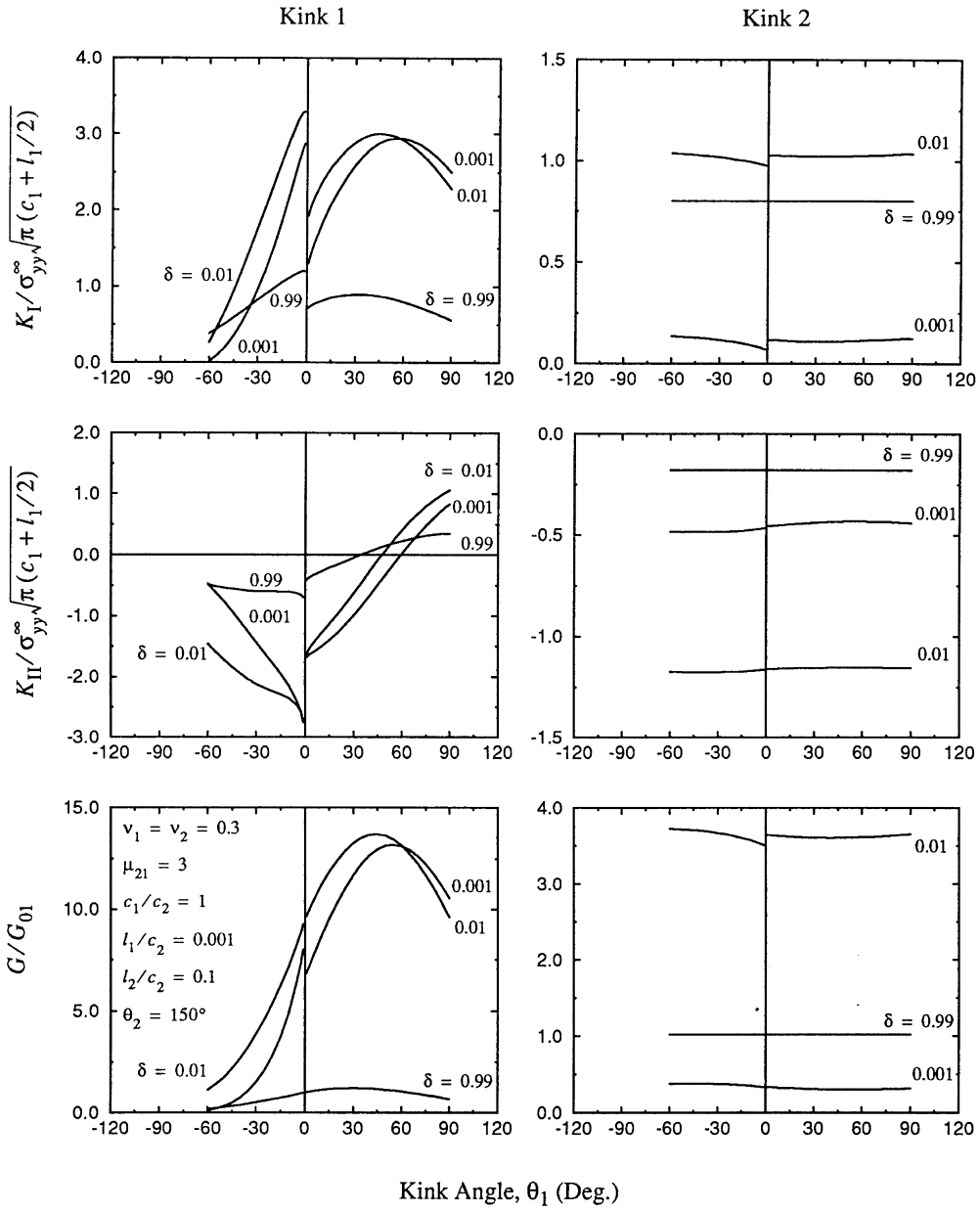

Fig. 9. Dependence of the SIFs and the energy release rate on the distance parameter δ of two kinked interfacial cracks containing equal interfacial parts and unequal kinks.

The complex curves of Fig. 9 result in fracture predictions quite different from the symmetric case. A most obvious difference is that it is possible for θ_{cr} to increase with $1/\delta$ if the infinitesimal kink extends into S_1. Second, the critical stress to cause extension of the infinitesimal kink is lower in the case of $\delta = 0.01$ compared to the case of $\delta = 0.001$, regardless of whether the kink extends into S_1 or S_2. Third, the finite kink generally experiences $\tilde{K}_I$ and $\tilde{G}$ values smaller than the maxima experienced by the infinitesimal kink, implying that the infinitesimal kink will extend before the finite kink can do so.

When the fracture toughnesses are taken into account, there can be significant discrepancies between the predictions of the maximum K_I and the maximum G criterion. Using the same parameters as in Section 5.2.2, i.e., $K_{IC,2}/K_{IC,1} = 1.43$ and $G_{C,2}/G_{C,1} = 0.68$, the predictions of the critical angles and stresses are shown in Fig. 10. For the critical angles, the two criteria agree approximately when $\delta = 0.01$ and 0.001 and disagree entirely for $\delta = 0.99$ and 0.1. Unlike the symmetric case, both criteria predict that the infinitesimal kink tends to leave the interface and approach the finite kink when $\delta = 0.01$ and 0.001. For the critical stresses, the largest discrepancy, which is of the order of 10%, also occurs at the larger values of δ, i.e. 0.99 and 0.1. Similar to the symmetric case, the stresses predicted by the maximum G criterion are smaller than those predicted by the maximum K_I criterion.

6. Conclusions

A model for two strongly interacting kinked interfacial cracks lying between two dissimilar isotropic materials is generalized from the previous model for a single crack. For two sets of Dundurs parameters (corresponding to $\mu_{21} = 3, 100$, $\nu_1 = \nu_2 = 0.3$), a symmetric and an asymmetric crack configuration under the plane strain conditions are studied. The focus is on the effect of interaction on the stress intensity factors, the energy release rates, and the predictions of the kink angles and the critical stresses using the maximum G and the maximum K_I criteria. The remote loading consists of a tensile stress normal to the material interface. Numerical examples are given using the following fracture toughness ratio of the two materials: $K_{IC,2}/K_{IC,1} = 1.43$ and correspondingly $G_{C,2}/G_{C,1} = 0.68$. The interface toughness is assumed to be at least as tough as the less tough of the two materials.

For the symmetric crack configuration, the kink angle corresponding to maximum K_I or G in the compliant material decreases with interaction. For a kink of a given angle in the stiff material, interaction increases the mode I mixity. In the compliant material, the general trend is for interaction to also increase the mode I mixity if the kink angles are small, but to reduce it if the kink angles are large. When the crack configuration is asymmetric, strong interaction may introduce complex effects. For instance, when an infinitesimal kink interacts with a finite kink, the angle of the infinitesimal kink at which K_I or G reaches its maximum in the compliant material increases with interaction. Generally, the finite kink also experiences greater shielding in both the stress intensity factors and the energy release rate than the infinitesimal kink.

It is shown that interaction can change the kinking behavior completely, i.e. from kinking into the compliant material to extending along the interface. These exist, however, discrepancies in the predictions of the maximum G and the maximum K_I criteria. When there is no interaction or only moderate interaction, the interface cracks in the symmetric configuration kink into the compliant

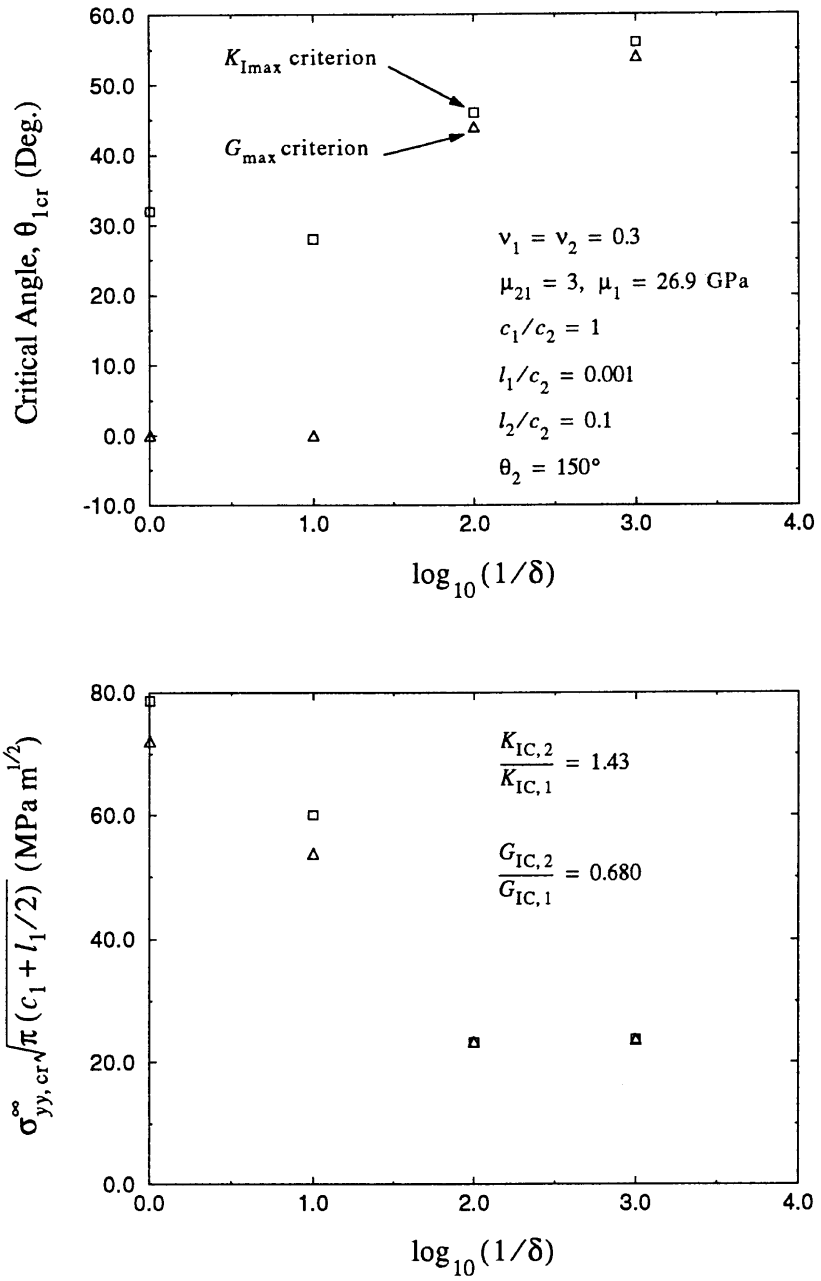

Fig. 10. Effect of interaction on the critical angle and the critical stress predictions, and discrepancies between the maximum K_I criterion and the maximum G criterion. The asymmetric crack configuration consists of equal interfacial parts and unequal kinks.

material according to the maximum K_I criterion while they remain in the interface according to the maximum G criterion. For the asymmetric configuration consisting of equal main cracks, one with an infinitesimal kink and the other a finite kink, a similar contradiction is predicted for the crack with the infinitesimal kink. On the other hand, when strong interaction exists both criteria predict that the kinks in the symmetric configuration stay in the interface, while the kink in the asymmetric configuration leaves the interface to approach the other kink. In general, the details of the discrepancies will be dependent on the crack configuration, the Dundurs parameters, and the ratios of the fracture toughnesses.

Acknowledgements

The author gratefully acknowledges the support of the Office of Naval Research in this investigation (Contract No. N00014-92-J-1203). The computational work is done on the Cray J90 supercomputer at the College of Engineering and Technology, University of Nebraska-Lincoln.

Appendix A

For Problem 1, the potentials $\Phi_j^\infty(z)$ and $\Psi_j^\infty(z)$ $(j=1,2)$ due to the remote loading are independent of position z. In view of (5) and (6), they can be written as:

$$\Phi_1^\infty = \frac{\sigma_{yy}^\infty + \sigma_{xx1}^\infty}{4}, \tag{A1}$$

$$\Psi_1^\infty = \frac{\sigma_{yy}^\infty - \sigma_{xx1}^\infty}{2} + i\sigma_{yx}^\infty, \tag{A2}$$

$$\Phi_2^\infty = \frac{\sigma_{yy}^\infty + \sigma_{xx2}^\infty}{4} + i\frac{\alpha-\beta}{1-\alpha}\sigma_{yx}^\infty, \tag{A3}$$

$$\Psi_2^\infty = \frac{\sigma_{yy}^\infty - \sigma_{xx2}^\infty}{2} + i\sigma_{yx}^\infty, \tag{A4}$$

where α and β are Dundurs' parameters:

$$\alpha = \frac{\mu_2(\kappa_1+1)-\mu_1(\kappa_2+1)}{\mu_2(\kappa_1+1)+\mu_1(\kappa_2+1)}, \quad \beta = \frac{\mu_2(\kappa_1-1)-\mu_1(\kappa_2-1)}{\mu_2(\kappa_1+1)+\mu_1(\kappa_2+1)}. \tag{A5}$$

In (A1)–(A4), it can be shown by continuity of the displacement gradient across the interface that σ_{xx1}^∞ is related to σ_{xx2}^∞, i.e.:

$$\sigma_{xx2}^\infty = \frac{4\beta-2\alpha}{1-\alpha}\sigma_{yy}^\infty + \frac{1+\alpha}{1-\alpha}\sigma_{xx1}^\infty, \tag{A6}$$

where it is further assumed that $\sigma_{xx2}^\infty = -\sigma_{xx1}^\infty$. The above equation implies that the x-direction stresses cannot be specified independently if constant potentials are assumed.

For Problem 2 or 3, the potentials $\Phi_j^{\perp}(z)$ and $\Psi_j^{\perp}(z)$ due to an edge dislocation at z_0 in S_1 can be written as (see, e.g. Mukai et al., 1990):

$$\Phi_1^{\perp}(z) = \frac{A}{z-z_0} + \frac{\alpha-\beta}{1+\beta}\frac{A}{z-\overline{z_0}} + \frac{\alpha-\beta}{1+\beta}\frac{\bar{A}(z_0-\overline{z_0})}{(z-\overline{z_0})^2}, \tag{A7}$$

$$\Psi_1^{\perp}(z) = \frac{\bar{A}}{z-z_0} + \frac{A\overline{z_0}}{(z-z_0)^2} + \frac{\alpha+\beta}{1-\beta}\frac{\bar{A}}{z-\overline{z_0}} - \frac{\mathrm{d}}{\mathrm{d}z}\left[z\left(\frac{\alpha-\beta}{1+\beta}\frac{A}{z-\overline{z_0}} + \frac{\alpha-\beta}{1+\beta}\frac{\bar{A}(z_0-\overline{z_0})}{(z-\overline{z_0})^2}\right)\right], \tag{A8}$$

$$\Phi_2^{\perp}(z) = \frac{1+\alpha}{1-\beta}\frac{A}{z-z_0}, \tag{A9}$$

$$\Psi_2^{\perp}(z) = \frac{1+\alpha}{1+\beta}\frac{A(\overline{z_0}-z_0)}{(z-z_0)^2} + \frac{1+\alpha}{1+\beta}\frac{\bar{A}}{z-z_0} - \frac{\mathrm{d}}{\mathrm{d}z}\left[z\left(\frac{1+\alpha}{1-\beta}\frac{A}{z-z_0}\right)\right], \tag{A10}$$

where $A = \mu_1 \mathrm{e}^{i\theta}\{[u_r]+i[u_\theta]\}/i\pi(\kappa_1+1)$ characterizes the edge dislocation; e is the exponential, (r, θ) the usual polar coordinates, and $[u_r]$, $[u_\theta]$ the displacement jumps in the radial and tangential directions. Also, the overhead bar denotes the complex conjugate.

References

Clements, D. L. (1971) A crack between dissimilar anisotropic media. *International Journal of Engineering Science* **9,** 257–265.

England, A. H. (1965) A crack between dissimilar media. *Journal of Applied Mechanics* **32,** 400–402.

Erdogan, F. (1962) On the stress distribution in plates with collinear cuts under arbitrary loads. *Proceedings of the Fourth U.S. National Congress of Applied Mechanics* **1,** 547–553.

Erdogan, F. (1965) Stress distribution in bonded dissimilar materials with cracks. *Journal of Applied Mechanics* **32,** 403–410.

Gerasoulis, A. (1982) The use of piecewise quadratic polynomials for the solution of singular integral equations of Cauchy type. *Computers and Mathematics with Applications* **8,** 15–22.

He, M. Y. and Hutchinson, J. W. (1989) Kinking of a crack out of an interface. *Journal of Applied Mechanics* **56,** 270–278.

Isida, M. and Noguchi, H. (1994) Distributed cracks and kinked cracks in bonded dissimilar half planes with an interface crack. *International Journal of Fracture* **66,** 313–337.

Kang, K. J. (1994) Criteria for kinking out of interface crack. *Engineering Fracture Mechanics* **49,** 587–598.

Lo, K. K. (1978) Analysis of branched cracks. *Journal of Applied Mechanics* **45,** 797–802.

Malyshev, B. M. and Salganik, R. L. (1965) The strength of adhesive joints using the theory of cracks. *International Journal of Fracture Mechanics* **1,** 114–118.

Miller, G. R. and Stock, W. L. (1989) Analysis of branched interface cracks between dissimilar anisotropic media. *Journal of Applied Mechanics* **56,** 844–849.

Mukai, D. J., Ballarini, R. and Miller, G. R. (1990) Analysis of branched interface cracks. *Journal of Applied Mechanics* **57,** 887–893.

Muskhelishvili, N. I. (1953) *Some Basic Problems of the Mathematical Theory of Elasticity*. Noordhoff, Groningen.

Niu, J. and Wu, M. S. (1997) Strong interactions of morphologically complex cracks. *Engineering Fracture Mechanics*, **57,** 665–687.

Obata, M., Nemat-Nasser, S. and Goto, Y. (1989) Branched cracks in anisotropic elastic solids. *Journal of Applied Mechanics* **56,** 858–864.

Raju, I. S. and Dattaguru, B. (1995) Review of methods for calculating fracture parameters for interface crack problems.

In *Computational Mechanics* '95, ed. S. N. Atluri, G. Yagawa and T. A. Cruse, **2,** 2020–2026. Springer-Verlag, Hiedelberg.

Rice, J. R. and Sih, G. C. (1965) Plane problems of cracks in dissimilar media. *Journal of Applied Mechanics* **32,** 418–423.

Yuuki, R., Liu, J. Q., Xu, J. Q., Ohira, T. and Ono, T. (1994) Mixed mode fracture for an interface crack. *Engineering Fracture Mechanics* **47,** 367–377.

Williams, M. L. (1959) The stresses around a fault or crack in dissimilar media. *Bulletin of the Seismological Society of America*. **49,** 199–204.

Zhao, L. G. and Chen, Y. H. (1994) Interaction of multiple interface cracks. *International Journal of Fracture* **70,** R53–R62.

Zhao, L. G. and Chen, Y. H. (1995) Interaction between an interface crack and a parallel subinterface crack. *International Journal of Fracture* **76,** 279–291.